PCCP

Experimental and theoretical CO_2–He pressure broadening cross sections

F. Thibault,* B. Calil, J. Boissoles and J. M. Launay

UMR 6627 du CNRS, P.A.L.M.S. (Physique des Atomes, Lasers, Molécules et Surfaces), Université de Rennes I, Campus de Beaulieu, 35042 Rennes Cedex, France.
E-mail: Franck.Thibault@univ-rennes1.fr

Received 1st August 2000, Accepted 6th October 2000
First published as an Advance Article on the web 3rd November 2000

We present experimental and theoretical results for the CO_2–He pressure broadening coefficients. Linewidths have been measured for the ν_3 bands of CO_2 in helium baths from 123 to 760 K with a Fourier transform interferometer. Close coupling calculations were performed with the MOLCOL program and with the most recent available potential energy surface (PES) of Negri *et al.* (*J. Chem. Phys.*, 1999, **111**, 6439). Generalised pressure broadening cross sections were then deduced and averaged over Maxwell–Boltzmann kinetic energy distributions to provide the thermally averaged linewidths. Theoretical calculations are in rather good agreement with the experimental data. In addition, we examine the effect of the radiation–matter interaction tensor order on the linewidths. Total inelastic cross sections obtained with the empirical PES of Beneventi *et al.* (*J. Chem. Phys.*, 1988, **89**, 4671) and with the *ab initio* PES of Yan *et al.* (*J. Chem. Phys.*, 1998, **109**, 10284) are also compared to those obtained with the *ab initio* PES of Negri *et al.*

I Introduction

Rovibrational spectra of the isolated carbon dioxide molecule are well known. It is therefore possible to study the modifications induced by the surrounding molecules. Knowledge of CO_2 lineshape parameters is important for a number of practical reasons. Since CO_2 is present in numerous planetary atmospheres, lineshape information allows atmospheric temperatures and density profiles to be deduced from remote sensing data. CO_2 spectra are also used to characterise combustion gases. Moreover the gain in a CO_2 laser depends on the lineshape and hence on the diluents. Additionally, pressure broadening and line shift measurements are amongst a number of tools theorists use to test both the intermolecular PESs, and the techniques for calculating transfer between atoms (or molecules) and molecules. The difficulty, as with much other experimental information, is that the spectrum is of a bulk sample.

As confirmed recently[1–3] in the case of the Ar–CO_2 system, pressure broadening cross sections contain useful information on the PES. However, due to the time consuming calculations that would have been necessary, these data were not included in the least-squares process to obtain the PESs. The authors checked *a posteriori* that their PESs give accurate line broadening coefficients.[3]

The particular case of CO_2 in interaction with helium has been the subject of considerable research and is the scope of the present paper. A complete He–CO_2 empirical potential surface was first derived by Keil and Parker[4] from a combined multiproperty analysis of available data. Three years later, Beneventi *et al.*[5] presented an improved surface based on new experimental data. However these works were limited by the infinite order sudden (IOS) approximation and by the lack of experimental observation of $HeCO_2$ bound levels. Weida *et al.*[6] reported the first IR spectrum of the $HeCO_2$ van der Waals molecule and in turn showed from predictions of close coupling (CC) calculations based on the PES of Beneventi *et al.*[5] that this potential is too isotropic in the region of the potential minimum. More recently two *ab initio* PES of the $HeCO_2$ van der Waals complex have been reported.[7,8] They were both determined using the fourth order Moller–Plesset (MP4) perturbation theory. In these studies, all the calculations were carried out using the Gaussian suite of programs 94 and 96. As expected the shapes of these surfaces are very similar.

In the impact approximation,[9,10] pressure broadening coefficients are calculated from the *S*-matrix elements for binary collisions. Full CC calculations of the pressure broadening coefficients have been carried out for a few prototype systems such as CO–He.[11,12] Less accurate quantal theoretical methods like the IOS approximation or the coupled states (CS) approximation have been more widely used[9,10] especially for more complicated systems. In particular, Green[13] applied the IOS method to the ν_2 bending band of CO_2 in helium. However, Pack[14] showed that in the cases of CO_2–He and CO_2–Ar, despite the small rotational spacing, the IOS predictions were inaccurate, at least for high rotational levels. Moreover, even the CS approximation departs from CC calculations for CO_2–Ar.[15]

In our laboratory, we have previously measured He–CO_2 pressure broadening cross sections at 296[16,17] and 193 K.[18] In the present work we extend these measurements to the ν_3 band of CO_2 down to 120 K and up to 760 K and compare all these results with CC predictions for rotational quantum numbers smaller than 20 for which CC calculations are not too expensive. As we believe that these are the first CC calculations for this system we also present results for Raman Q lines. In addition, we will show that the "random phase approximation"[19,20] applied to the line broadening problem[21,22] is quite accurate for this system. Finally, we will briefly compare predictions based on the PES of Negri *et al.*[8] with those obtained with the PESs of Beneventi *et al.*[5] and Yan *et al.*[7]

II Experimental procedure and data reduction

A Fourier transform spectrometer (Bruker IFS 120 HR), equipped with a KBr beam-splitter, a globar source, a liquid

 DOI: 10.1039/b006224n

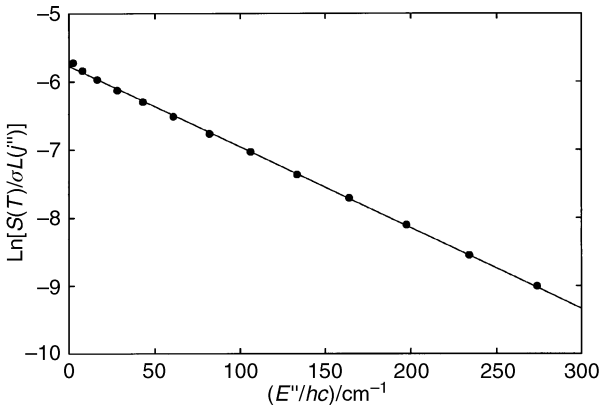

Fig. 1 Check of the temperature of an experimental spectrum recorded at 123 K from the line intensity (see eqn. (1)). The slope gives $T = 120.9$ K.

nitrogen cooled InSb detector, and operated under vacuum was used. The spectral range was limited by an optical bandpass filter from 2100 to 2550 cm^{-1} and each spectrum was the average result of 60 interferograms. The resolution varied from 0.002 to 0.032 cm^{-1} as the pressure increased. The instrument offers several possibilities of accessing the optical beam. For studies limited to short optical path lengths, less than 30 cm, we use the sample compartment of the spectrometer: cells are integrated under vacuum in the spectrometer. Commercially available carbon dioxide and helium (Air Liquide) were used for the gaseous mixtures.

A Low temperature experiments

A single path cell with a baseline of 160 mm was used. The cell is made of a double-walled stainless-steel tube which allows the circulation of cryogenic fluid cooled by liquid nitrogen and the cell is surrounded by several dozen superinsulation layers. The input and output windows were both made of sapphire disks: the internal ones were at cell temperature and the external ones were kept at room temperature by means of water circulation to avoid any condensation. The temperatures were monitored by a copper–constantan thermocouple probe connected to a Chauvin–Arnoux cold temperature control system. For control, the cell temperature was directly checked by a platinum resistive thermal probe. Differences less than 2 K were obtained.

The mixtures were prepared in the cell at room temperature. First a certain quantity of CO_2 was introduced, and its pressure was measured using a Datametrics 590 capacitance manometer (0–1000 Torr, 3 scales). After evacuating the connecting tubing, the cell was filled with helium, and the total pressure was measured. CO_2 concentrations in the mixtures never exceeded 1%. Once the cell was hermetically sealed, it was cooled. Spectra were then recorded at 193, 160 and 123 K. This procedure was repeated five times for helium pressures at room temperature (294 K) in the range 225–600 Torr. Note that at the lowest temperature investigated, the CO_2 gas phase was just under the sublimation curve.

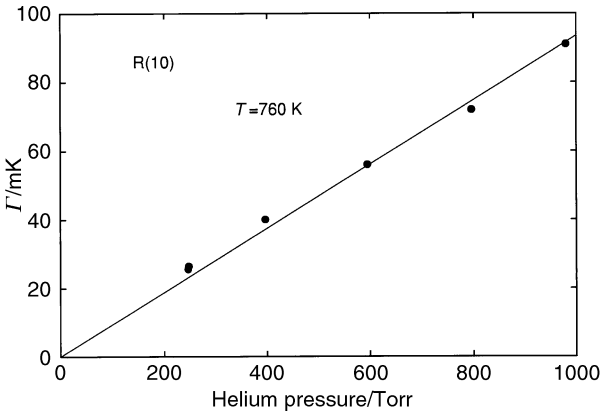

Fig. 2 Variation of the collisional width of the R(10) line with the helium pressure at 760 K. The slope of the straight line gives the normalised HW-M (see eqn. (2)). (Recall that 1 mK = 1×10^{-3} cm^{-1}).

B High temperature experiments

The oven is composed of a cylindrical cavity surrounded by an important mass of metal, which homogenises the temperature in order to minimise the temperature gradients in the cell. Two articulated ceramic bands were used to heat the metallic mass, with temperatures of up to 1070 K possible. The system was wrapped in an insulating material, 25 mm thick, composed of ceramic fibers, stiffened by binders and liquid ceramic gums. To reduce the loss of IR radiation to the exterior, a copper cylinder cooled by water surrounded the oven. A diaphragm located at the focal point between the cell and the detector limits the field of view for the thermal radiation from the hot cell. A half beam diaphragm coupled with the corner cube mirror suppressed the modulated retroreflected beam emitted by the hot cell.

Temperature measurements and regulation were achieved by two thermocouples of type K. The temperature was controlled by an autoadaptative logical circuit: definition, integration and differentiation in T. This system allows a regulating scale between 300 and 1070 K, with residual oscillations less than 1 K. This system, regulated in temperature, can be dismounted in order to insert an optical cell of length up to 20 cm. The windows of the high temperature optical cell are in sapphire and sealed using hélicoflex (CEFILAC) joints covered by silver. The cell can be fed by a special high temperature valve mounted on the cell to avoid inhomogeneities in the gas through exchange with the exterior. In the present work, two cells of optical length 35 and 192 mm were used in order to investigate respectively low and high rotational quantum numbers j of the rovibrational lines. For each absorption path length and at each temperature (565 and 760 K) six mixtures were studied with helium pressures varying from 200 to about 900 Torr and CO_2 pressure varying from 1 to 5% of the total pressure.

C Data treatment

The temperature was checked as follows. The intensity $S(T)$ of a line at temperature T is given approximately by:

$$S(T) = K\sigma L(j'')\exp\left(-\frac{E''}{k_B T}\right) \quad (1)$$

where $L(j'')$ is the Hönl–London factor, E'' the initial energy level of the transition which occurs at wavenumber σ and K is assumed to be temperature independent. From a logarithm plot of $S(T)/\sigma L(j'')$ *vs.* E'' the temperature was deduced. A maximum deviation of 2 K was found for the lowest temperature samples at 123 K (Fig. 1).

To measure the widths of the ν_3 band lines we had previously subtracted the Lorentzian contribution of all other bands of all CO_2 species provided by the Hitran database[23] in the range 2300–2400 cm^{-1}. This decontamination is especially important at high temperature near the centre of the ν_3 band where hot bands contribute significantly to the absorption.

Linewidths were measured with the Peakfit program of Grams™ assuming a Lorentzian profile and also with the code provided by Michel Carleer [Université Libre de Bruxelles] specially developed for Bruker spectra assuming a Voigt profile (this program also takes into account the instrumental function). Slight deviations of the order of 1% were

found. Pressure reduced half widths at half maximum (HWHM) were deduced from the slope of the line joining the measured widths since the collisional broadening part of the observed width of a line is given by:

$$\Gamma = 2P_p\gamma^0 \tag{2}$$

where P_p is the pressure of the perturber atoms (*i.e.* helium) and γ^0 the normalised (per atmosphere) HWHM (Fig. 2 gives an illustration).

Uncertainties on the normalised HWHM are estimated to be of the order of 5% but are slightly greater for low j values at high temperatures due to the decontamination procedure.

III Linewidth calculations

In the impact and binary collision approximations,[24–27] the rotationally invariant line shape cross section of an isolated line may be calculated in terms of S-matrix elements for the molecular collisions involved. In the CC scheme where the total angular momentum $\boldsymbol{J} = \boldsymbol{j} + \boldsymbol{l}$ of the system is conserved, these cross sections have the form:[27]

$$\begin{aligned}\sigma^{(n)}(\chi_a\chi_b; E_{kin}) = \left(\frac{\pi}{k^2}\right) \sum_{J_a J_b l l'} (2J_a+1)(2J_b+1) \\ \times \begin{Bmatrix} j_a & n & j_b \\ J_b & l & J_a \end{Bmatrix} \begin{Bmatrix} j_a & n & j_b \\ J_b & l' & J_a \end{Bmatrix} \\ \times [\delta_{ll'} - \langle \chi_a l' | S^{J_a}(E_{kin}+E_{j_a}) | \chi_a l\rangle \\ \times \langle \chi_b l' | S^{J_b}(E_{kin}+E_{j_b}) \chi_b l\rangle^*]\end{aligned} \tag{3}$$

where n is the tensor order of the radiative transition (0 for isotropic Raman, 1 for IR, 2 for anisotropic Raman). χ_a, χ_b label the two states involved in the spectroscopic transition ($\chi \equiv vj$ if only vibrational and rotational quantum numbers are needed) and $E_{kin} = (\hbar^2k^2/2\mu)$ is the center of mass kinetic energy; note that the CC S-matrix elements which are expressed in the total angular momentum representation are evaluated at the same kinetic energy and not at the same total energy (denoted hereafter E_T, $E_T = E_{kin} + E_j$). l and l' are the relative orbital angular momentum quantum numbers before and after collision.

A transformation can be performed to obtain the irreducible components[28,29] of the S-matrix from the expression of the S-matrix elements in the total angular momentum representation scheme:

$$\begin{aligned}S^{(x)}_{j'l'jl} = \sum_J (-1)^{J+j+l'+x}(2J+1)(2x+1)^{1/2} \\ \times \begin{Bmatrix} j & l & J \\ l' & j' & x \end{Bmatrix} S^J_{j'l'jl}\end{aligned} \tag{4}$$

where $\boldsymbol{x} = \boldsymbol{j}' - \boldsymbol{j} = \boldsymbol{l} - \boldsymbol{l}'$ is the angular momentum transferred during the collision. With the help of this coupling scheme the generalised cross sections can be written as:[28,30]

$$\begin{aligned}\sigma^{(n)}(\chi_a\chi_b; E_{kin}) = \left(\frac{\pi}{k^2}\right)(-1)^{j_a+j_b+n} \\ \times \sum_x (-1)^x \begin{Bmatrix} j_a & j_a & x \\ j_b & j_b & n \end{Bmatrix} \\ \times \sum_{ll'} [(2l+1)\delta_{ll'}\delta_{x0}\sqrt{(2j_a+1)(2j_b+1)} \\ - \langle \chi_a l' | S^{(x)}(E_{kin}+E_{j_a}) | \chi_a l\rangle \\ \times \langle \chi_b l' | S^{(x)}(E_{kin}+E_{j_b}) | \chi_b l\rangle^*]\end{aligned} \tag{5}$$

The advantage of this expression has already been discussed[31] and this is the form we have used in this work.

One can easily check the following relationship between the tensorial relaxation pressure broadening cross sections of order 0 and the usual inelastic cross sections:

$$\sigma^{(0)}(jj) = \sum_{j' \neq j} \sigma(j \to j') \tag{6}$$

The expression (5) for the line shape cross section accounts for inelastic events, reorientation and purely dephasing contributions. Nevertheless, a practical separation can be performed[24,26,32,33] which results from the unitarity of the S-matrix:

$$\sigma^{(n)}(\chi_a\chi_b; E_{kin}) = \sigma_{in}(\chi_a\chi_b; E_{kin}) + \sigma^{(n)}_{dep}(\chi_a\chi_b; E_{kin}) \tag{7}$$

where σ_{in}, which is independent of the order of the tensor, is the average total inelastic rotational state-to-state cross section in the upper and lower vibrational levels, while σ_{dep} is the dephasing cross section which is n dependent and complex. Let us recall that the dephasing part is zero in the case of purely rotational isotropic Raman Q lines (Eqn. (6)). Nevertheless, vibrational dephasing can, in fact, be safely ignored in most cases[9,10] and this is certainly true for CO_2–He since no significant vibrational effect has been observed to date in the linewidths.[16,34] In conjunction with the assumption that all orientations are equivalent, this statement partly justifies a random phase approximation which allows neglect[21,22] of the second contribution of the right hand side of eqn. (7). Clearly, within the RPA we are left with:

$$\sigma^{(n)}_{ab} = \frac{1}{2}\left(\sum_{j_a' \neq j_a} \sigma(v_a\, j_a \to v_a\, j_a') + \sum_{j_b' \neq j_b} \sigma(v_b\, j_b \to v_b\, j_b')\right) \tag{8}$$

The Lorentzian HWHM, associated with a sample at temperature T, is obtained by assuming the colliding particles have a Maxwellian thermal distribution:[27]

$$\begin{aligned}\gamma_{ab}(T) &= n_p\langle v\sigma^{(n)}(\chi_a\chi_b; E_{kin})\rangle \\ &\equiv n_p\,\bar{v}\langle\sigma^{(n)}(\chi_a\chi_b; E_{kin})\rangle\end{aligned} \tag{9}$$

with

$$\begin{aligned}\langle\sigma^{(n)}(\chi_a\chi_b; E_{kin})\rangle = \left(\frac{1}{k_BT}\right)^2 \\ \times \int_0^\infty E_{kin}\,\sigma^{(n)}(\chi_a\chi_b; E_{kin})\exp(-E_{kin}/k_BT)\mathrm{d}E_{kin}\end{aligned} \tag{10}$$

where n_p is the density of the perturbers and $\bar{v} = \sqrt{(8k_BT/\pi\mu)}$ is the mean relative velocity.

In order to derive such relaxation cross sections, we computed the S-matrix elements with the MOLCOL[35] computer program. The body-frame CC equations were solved with the Johnson[36] log-derivative propagator. The propagation was carried out between a minimum distance of 3.5 a_0 to a maximum distance of 50 a_0 with a constant step size corresponding to 8 points per half wavelength for the open channel of highest kinetic energy (in the asymptotic region). All energetically open rotational levels, and at least four closed rotational levels, were included at each total energy. The summation over the partial waves was stopped when the maximum elastic probability was converged to better than 5×10^{-4} (this gives a relative error of the order of 1% for the highest elastic cross sections and much less for the inelastic state to state cross sections); for example 150 (75 for each parity) partial waves were included for a run of MOLCOL[35] at a total energy of 300 K.†

We generated for the ground state a first set of 29 total energies ranging from 5 to 2000 K and a second set of at least

† Here, and in the following, energies are expressed in K with 1 K = 1.380 658 × 10^{-23} J.

12 total energies for each rotational level of the upper vibrational level. The three last *S*-matrix files of both sets corresponding to total energies of 1000, 1500 and 2000 K were calculated using the CC method in conjunction with the sudden energy approximation where the rotational energy level spacing is ignored. This allows us to obtain all *S*-matrix elements from only two runs of MOLCOL,[35] one for each vibrational level, in total energy or in kinetic energy since at that level of approximation no distinction is made between the kinetic and the total energy.

A separate code from MOLCOL,[35] took as input one file of each set for the IR lines (one is sufficient for the Q lines) and generated the generalised cross sections (eqn. (5)). Finally the thermal average was performed by using common routines of the NAG library (cubic-spline, quadrature . . .). We have mainly used the most recent He–CO_2 intermolecular potential $V(R,\theta)$ of Negri *et al.*[8] where R is the distance between the C and He atoms and θ the angle between the $\boldsymbol{R}$ vector and the molecular axis. This potential was expanded over 16 Legendre polynomials $P_\lambda(\cos\theta)$ with even λ (P_0, $P_2 \cdots P_{30}$). The expansion coefficients were computed using 40-points Gauss–Legendre quadrature in θ between 0 and π restricted to 20-points between 0 and $\pi/2$ because of symmetry. This PES, like those of Beneventi *et al.*[5] and Yan *et al.*,[7] has no vibrational dependence so lineshift calculations are not reported. In fact, they are expected to be very small for the IR ν_3 band, at least at room temperature.[16]

The CO_2 rovibrational levels of the ground state 00^00 and of the 00^01 state (with the standard notation $v_1v_2^{l_2}v_3$) are taken from the Hitran data bank.[23]

IV Results and discussion

A Comparison between experimental IR linewidths and CC calculations

The experimental and theoretical results for the R lines of the IR active ν_3 band are presented in graphical form in Fig. 3. The experimental HWHM at 296 K are smoothed values deduced from ref. 16 and 17. The new results at 193 K can be easily compared with those previously obtained in the ν_2 and $3\nu_3$ band of CO_2.[18] The overall agreement between CC and experimental results is satisfactory. The magnitude of the half widths as well as their general trends with rotational quantum number j and with temperature are well reproduced. The agreement is very good at 296 K and a little less satisfactory for the other temperatures. Note also that for our theoretical calculations an uncertainty of the order of 1% is estimated from the results provided by two different quadrature routines used to perform the thermal average.

While many experiments were performed at room temperature or even at higher temperatures (ref. 37, ref. 18 and 34 and references therein) very few were undertaken in the low temperature regime. The measured values of Brownsword *et al.*[34] suffer from a great scatter; in addition, their values at 160 K are too large compared to ours; this is also the case for their CO_2–Ar values at 160 K compared to the calculated ones of Roche *et al.*[3]

More theoretical than experimental studies were devoted to the CO_2–He pressure broadened cross sections[4,13,14] or related quantities.[38,39] However all these studies were carried out with the IOS approximation. Despite this, and the different PESs used, the results of these previous works are rather good. The values predicted by Pack[14] are 10% larger than our values and obviously fail to decrease at high j values; this is inherent in the sudden approximation which neglects rotational spacings whatever the kinetic energy. The values of Keil and Parker[4] are closer to ours at 300 K. We infer that these discrepancies are mostly due to the PESs rather than to the IOS approximation. Indeed, the latter approximation should

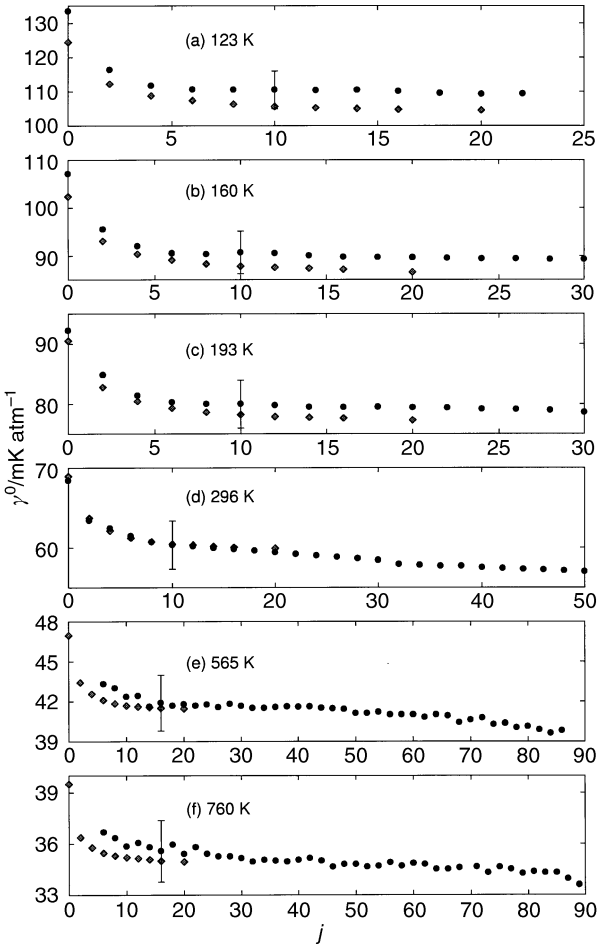

Fig. 3 Experimental (●) and calculated (◆) normalised per helium atmosphere HWHM *vs.* j at various temperature for R(j) lines. The vertical bars indicate an absolute error of 5%.

hold for this system, at least for low j values, because the rotational constant of CO_2 is very small ($B \approx 0.39$ cm^{-1}), the reduced mass is also small and the largest well depth is only 63 K. In addition, the variation of the pressure broadening cross sections with kinetic energy is quite small (see ref. 14 and below) for kinetic energies greater than 150 K; as a consequence also, in the thermal average only the pressure broadening cross sections of kinetic energies close to k_BT contribute significantly to the halfwidths.

From an experimental point of view, it is of practical interest to have a simple modelling of the variation of the HWHM with temperature. The following empirical law is commonly used:

$$\gamma^0(T) = \gamma^0(T_0)\left(\frac{T_0}{T}\right)^{\alpha} \qquad (11)$$

where T_0 is some reference temperature and α is positive when one works at constant pressure.

Khalil *et al.*[18] estimated a mean value of $\alpha = 0.7$ and Brownsword *et al.*[34] derived a value of $\alpha = 0.69 \pm 0.17$ from their low temperature measurements. Taking $T_0 = 300$ K, from Table II of Pack[14] one can derive a mean value $\alpha = 0.655 \pm 0.01$ for the low temperatures he had considered. Our findings show a slight decrease of α from 0.64 to 0.60 as j increases from 0 to 20. From Pack's Table II again, α is close to 0.6 in the range 600–800 K and our theoretical results show a slight variation from 0.59 to 0.57. Investigation by Brimacombe and Reid[37] in the range 300–508 K of the P(16) and P(32) lines of the 10 μm band of CO_2 provided a mean value of $\alpha = 0.58$ close to our results. Also, from our measurements one can simply show that α tends to 0.5 as j increases. This

behaviour is expected because as j increases the collisions are most sensitive to the repulsive part of the intermolecular potential and so the variation of the linewidths with temperature should tend to the gas kinetic theory limit behaviour (*i.e.* to $\alpha = 0.5$). This argument is reinforced for temperatures above room temperature.[14]

Finally, our results confirm the well known small variation with j of the pressure broadening coefficients, especially at high temperature where they approach a value independent of j which reflects the shallow attractive well of this system.

B Influence of the tensor order and validity of the RPA for the linewidths

In this section we investigate how the linewidths change with the tensor order of the radiative interaction; we also check the validity of the application of the RPA to the linewidths calculation. Calculations were performed for a single kinetic energy $\bar{E}_{kin} = (4k_B T/\pi)$ which corresponds to the mean relative velocity $\bar{v}$ at 296 K. The derived halfwidths $\bar{v}\sigma(\bar{E}_{kin})$ are plotted in Fig. 4. Note that the absolute error between these unaveraged values and the averaged ones is less than 1.5%. Fig. 4 shows that the influence of the order of interaction is only important for relatively low j values. Indeed, a detailed analysis of the 6j coefficients appearing in eqn. (5) indicates that they converge for a given x to a value which is independent of n for large j_a ($\geqslant$16) and equal to $1/2j + 1$ (in eqn. (5) the sign appearing before the 6j coefficients is the same for each line type). In consequence, as j increases the different species of halfwidths become closer. The "well" occurring near $j = 6$ for the Q(j) $n = 0$ halfwidths is not understood but such a variation has also been observed in the total inelastic cross sections calculated by Agrawal and Raff[38] for kinetic energies smaller than 650 K. This behaviour is also apparent for the R halfwidths estimated with the random phase approximation. This finding is expected since in this approximation an R(j) linewidth is the half sum of two Q linewidths. The good agreement between the estimated halfwidths and the Q(j) or real R(j) ones implies that elastic reorientations do not contribute significantly to the broadening process. As predicted by De Pristo and Rabitz[40] slight differences are only noticed for small j values.

To our knowledge no isotropic Raman linewidths have yet been measured, while S(j) linewidths have been measured by Herpin and Lallemand[41] at room temperature (295 K). Their results (when converted from mK Amagat^{-1} to mK atm^{-1}) are comparable to ours taking into account their large experimental uncertainties due to experimental difficulties. In addition, the comparison between Raman anisotropic Q(j) and S(j) HWHM indicates that the order of the tensor is more important than the Δj of the transitions.

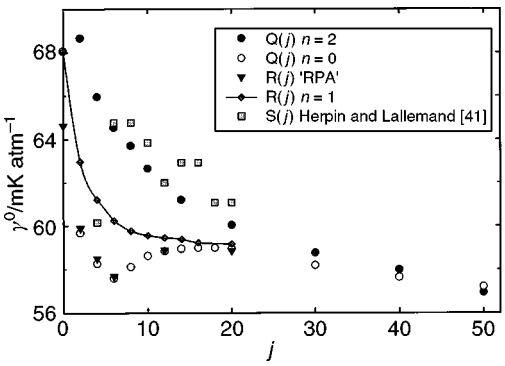

Fig. 4 Unaveraged pressure broadening cross sections for a kinetic energy $E_{kin}/k_B = 377$ K for tensor orders $n = 0$, 1, 2 and random phase approximation for IR R lines (eq. (8)). Also shown are the experimental results of Herpin and Lallemand[41] for Raman anisotropic S lines.

Finally, note that the HWHM calculated at high j values are in very good agreement with the experimental ones at 296 K plotted on Fig. 3. The order of magnitude is excellent as well as the small diminution of the HWHM with j which is not reproduced by Pack[14] or by Keil and Parker[4] within the IOS approximation.

C Influence of the PES

We have compared experimental linewidths with theoretical results obtained with the most recent *ab initio* surface.[8] Even if our theoretical predictions give the best agreement to date with experimental values on the whole, this test of that PES is rather disappointing, in particular at the lowest temperature of 123 K. Nonetheless, our experimental measurements at low temperature may suffer an unexplained bias and for instance they do not seem to sufficiently decrease as j increases. It was therefore interesting to try other surfaces. The *ab initio* PES of Yan *et al.*[7] and the empirical PES of Beneventi *et al.*[5] derived from a multiproperty fit of experimental data were used.

Yan *et al.*[7] have highlighted the differences between their *ab initio* potential which is close to the PES of Negri *et al.*[8] and the empirical one of Beneventi *et al.*[5] Table 1 and Fig. 5 recall the salient differences for the present comparison. The T-shaped minimum is the global minimum for each surface. The PES of Beneventi *et al.*[5] is the less deep but is the most attractive at large distances. A secondary minimum is found in the case of the *ab initio* potentials for the L-shaped structure. These secondary minima are separated from the global minimum by a repulsive barrier. The interconversion barrier gives the impression that the *ab initio* PESs[7,8] are more anisotropic (see Fig. 1 and 4 of ref. 7 and 8), this is only obvious in the most attractive directions. However, the well part of the PES of Yan *et al.*[7] is slightly more anisotropic than the well part of the PES of Negri *et al.*[8] The repulsive parts of these PESs are similar, the repulsive part of the PES of Negri *et al.*[8] being closer to the PES of Beneventi *et al.*,[5] which is expected to be accurate from the experimental data these authors had used to determine their surface. Finally, the bottom part of the "wall" is more anisotropic in the case of the empirical PES.

Linewidths are closely related to inelastic cross sections. For a purely rotational isotropic Raman Q branch, a pressure broadening cross section is equal to the sum of inelastic state-to-state cross sections out of the level involved in the Raman transition (see eqn. (6)); this remains valid for other types of transitions within the RPA[19,20] which we have confirmed to be correct for this system, at least for not too low j values.

It is unclear how sensitive the total inelastic cross sections are to the details of the PESs. Nevertheless, it is expected that for the highest kinetic energies the dominant interaction is assumed by the repulsive parts of the potentials which are quite similar. For lower kinetic energies the complete surface should be taken into account. In order to discriminate between the role of the repulsive part and the role of the well we have performed two calculations for each PES: one with the full surface and one by eliminating the well.

Table 1 Location and depth of the well in the directions 0°, 45° and 90° for the PESs of Beneventi *et al.*,[5] Yan *et al.*[7] and Negri *et al.*[8]

	Beneventi *et al.*[5]			Negri *et al.*[8]			Yan *et al.*[7]		
θ/degrees	0	45	90	0	45	90	0	39	90
R/Å	4.75	3.95	3.14	4.3	3.95	3.1	4.26	4.1	3.1
V_m/K	22.7	36.4	59	37.85	33.95	66.2	39.85	28.5	63.9

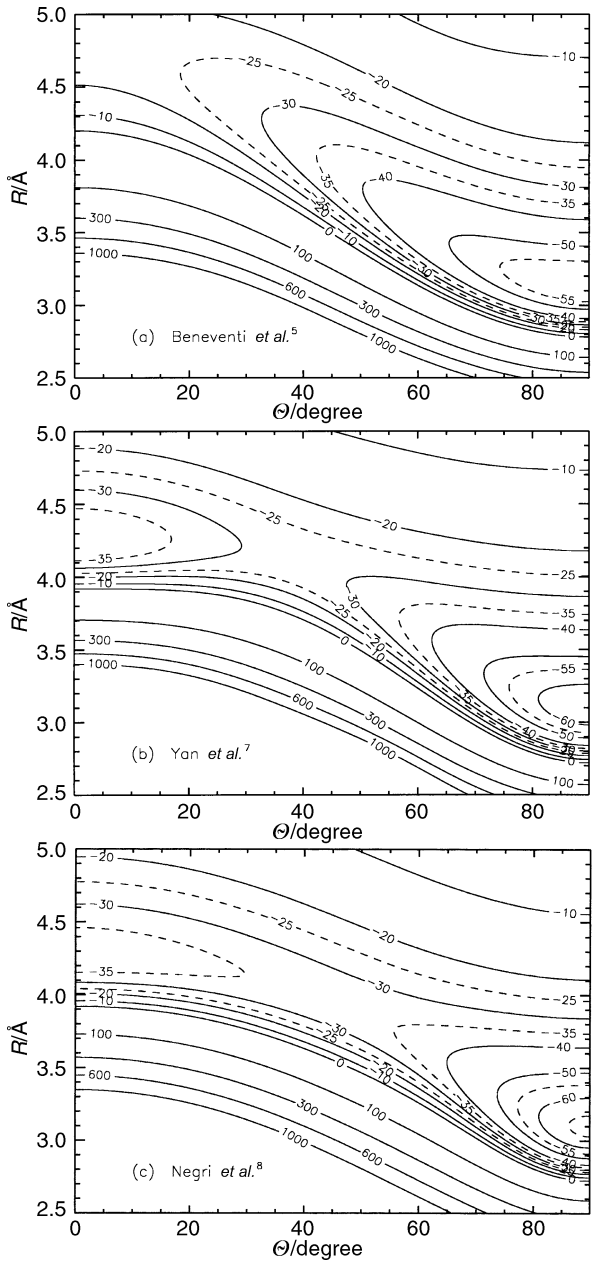

Fig. 5 Contour plots of the PES of Beneventi *et al.*[5] (a), Yan *et al.*[7] (b) and Negri *et al.*[8] (c). Contours are shown in K.

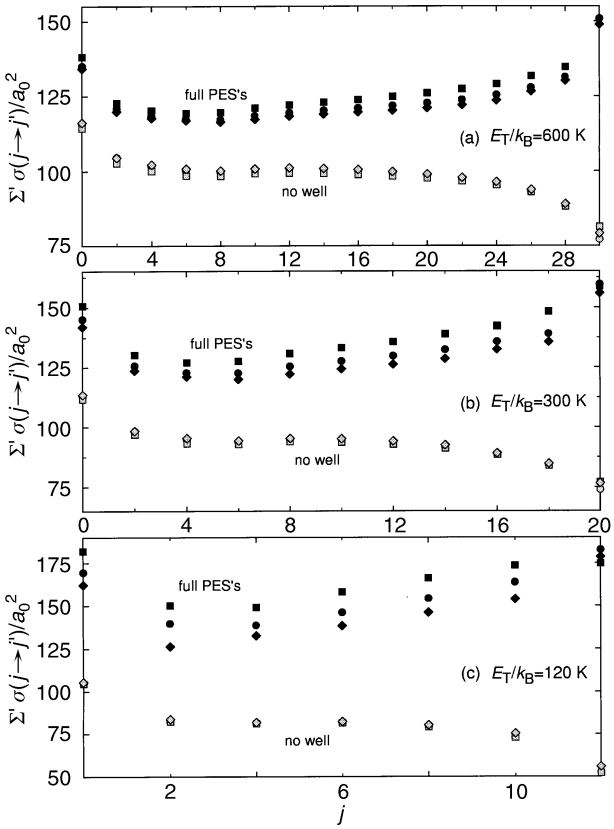

Fig. 6 Comparison of total inelastic state-to-state cross sections (in a_0^2) *vs.* j (the rotor angular momentum) for total energies E_T/k_B of (a) 600, (b) 300 and (c) 120 K, obtained with the PES of Negri *et al.*[8] (circles), Yan *et al.*[7] (diamonds) and with the PES of Beneventi *et al.*[5] (squares) with or without the well.

Fig. 6 compares the total inelastic cross sections obtained with the PES of Beneventi *et al.*,[5] Yan *et al.*[7] and Negri *et al.*[8] for three total energies. The overall agreement for the three total energies between the results obtained with the three surfaces is rather good when keeping the full PESs as well as when the wells are eliminating. For the two types of computations the deviations between the results obtained with the different PESs are nearly constant and quite small. These deviations are smaller in the case of the computations performed by eliminating the well. This implies that the observed differences, while taking into account the full PESs, are mainly due to the wells.

Since the repulsive (positive) part of the PES of Beneventi *et al.*[5] is expected to be accurate due to the experimental data used to fit it, the results found by eliminating the well of each *ab initio* surface give confidence in their own repulsive part.

Examination of Fig. 6 also allows us to make the following conclusions. The influence of the well diminishes as the kinetic energy increases as expected, but at the highest kinetic energy (600 K for $j = 0$) its contribution is still important ($\approx$20%). Calculations performed by eliminating the well show, for a given total energy, (Fig. 6) that the diminution of the sum of the inelastic cross sections is more rapid as j increases because the available kinetic energy decreases quadratically with j (inelastic cross sections converge to zero in that case: see ref. 42 for a classical argument). The same calculations also show for each j value that when the kinetic energy decreases (Fig. 6(a)–(c)) there is a monotonic decrease of the total inelastic cross sections which is not observed when the full PES is kept. These last comments reflect the neglect of long range forces and confirm[38] the great sensitivity of the sum of the inelastic cross sections to these forces when the full PES is considered.

A quite surprising consequence of this comparison between the three PESs is that linewidths derived from the empirical PES[8] should be in better agreement with the low temperature experimental values while linewidths derived from the PES of Yan *et al.*[7] should agree less well, although this PES has been successfully tested on $HeCO_2$ van der Waals spectra. Such a discrepancy had been already remarked in the case of CO_2–Ar.[1] However, as the temperature increases the predicted linewidths given by these PES should become closer.

V Conclusion

The present study has extended the available linewidth measurements of CO_2 perturbed by He over a wide range of temperature. Linewidths predicted from close coupling calculations with the *ab initio* potential energy surface of Negri *et al.*[8] agree with experimental results on the whole, at least for the limited set of calculated values, but deviations increase as the temperature decreases. Investigation of the matter–radiation interaction tensor order has been performed and has shown that this order is of non-negligible influence for low j values, contrary to the case of relatively high j values.

It would be worthwhile now to compare these calculations with new Raman measurements. In addition, CS calculations should be carried out for higher rotational quantum numbers since this approximate method is much less costly than the CC method.

Results obtained with three PESs have also been presented. They all lead to very similar results with deviations comparable to the experimental errors. This analysis also demonstrates the great sensitivity of the linewidths to the PES since the three potentials considered are globally similar. Measurements at lower temperatures where rotational resonances could be important should be undertaken as a better test of the influence of the well. The collisional cooling technique is well suited for this purpose. Further extension of the range of validity of the PESs based on different kinds of experimental data should also be performed.

Acknowledgements

F.T. thanks G. Bourhis (PALMS) for his assistance with the computational aspects of this work and Pr. C. Boulet (Laboratoire de Photophysique Moléculaire-Orsay) for the valuable comments he has made for the preparation of this manuscript.

B.K. thanks Michel Carleer (Laboratoire de Chimie-Physique Moléculaire-Université Libre de Bruxelles) for having provided him with his code "spectrav".

The calculations reported were partly performed on the SUN Enterprise 6500 of the "pole de calcul intensif" located in the University of Rennes.

References

1 C. Roche, A. Ernesti, J. M. Hutson and A. S. Dickinson, *J. Chem. Phys.*, 1996, **104**, 2156.
2 J. M. Hutson, A. Ernesti, M. M. Law, C. F. Roche and R. J. Wheatley, *J. Chem. Phys.*, 1996, **105**, 9130.
3 C. F. Roche, A. S. Dickinson, A. Ernesti and J. M. Hutson, *J. Chem. Phys.*, 1997, **107**, 1824.
4 M. Keil and G. Parker, *J. Chem. Phys.*, 1985, **82**, 1947.
5 L. Beneventi, P. Casavecchia, F. Vecchiocattivi, G. G. Volpi, U. Buck, Ch. Lauenstein and R. Schinke, *J. Chem. Phys.*, 1988, **89**, 4671.
6 M. J. Weida, J. M. Sperhac, D. J. Nesbitt and J. M. Hutson, *J. Chem. Phys.*, 1994, **101**, 8351.
7 G. Yan, M. Yang and D. Xie, *J. Chem. Phys.*, 1998, **109**, 10284.
8 F. Negri, F. Ancilotto, G. Mistura and F. Toigo, *J. Chem. Phys.*, 1999, **111**, 6439.
9 S. Green, in *Status and Future Developments in Transport Properties*, ed. W. A. Wakeham, Kluwer Academic, Dordrecht, 1992, p. 257.
10 A. Lévy, N. Lacome and C. C. Chackerian, Jr., in *Spectroscopy of the Earth's Atmosphere and Interstellar Medium*, ed. K. N. Rao and A. Weber, Academic, New York, 1992, p. 261.
11 J. Boissoles, C. Boulet, D. Robert and S. Green, *J. Chem. Phys.*, 1989, **90**, 5392.
12 M. M. Beaky, T. M. Goyette and F. C. De Lucia, *J. Chem. Phys.*, 1996, **105**, 3994.
13 S. Green, *J. Chem. Phys.*, 1989, **90**, 3603.
14 R. T. Pack, *J. Chem. Phys.*, 1979, **70**, 3424.
15 C. F. Roche, A. S. Dickinson and J. M. Hutson, *J. Chem. Phys.*, 1999, **111**, 5824.
16 F. Thibault, J. Boissoles, R. Le Doucen, J. P. Bouanich, Ph. Arcas and C. Boulet, *J. Chem. Phys.*, 1992, **96**, 4945.
17 J. Boissoles, F. Thibault, R. Le Doucen, V. Menoux and C. Boulet, *J. Chem. Phys.*, 1994, **101**, 6652.
18 B. Khalil, O. Cisse, G. Moreau, F. Thibault, R. Le Doucen and J. Boissoles, *Chem. Phys. Lett.*, 1996, **263**, 811.
19 H. S. W. Massey and C. B. O. Mohr, *Proc. R. Soc. London Ser. A*, 1933, **141**, 434; R. G. J. Fraser, H. S. W. Massey and C. B. O. Mohr, *Z. Phys.*, 1935, **97**, 740.
20 R. B. Bernstein, *Adv. Chem. Phys.*, 1966, **10**, 75.
21 A. E. DePristo, S. D. Augustin, R. Ramaswamy and H. Rabitz, *J. Chem. Phys.*, 1979, **71**, 850.
22 A. E. DePristo and H. Rabitz, *J. Quant. Spectrosc. Radiat. Transfer*, 1979, **22**, 65.
23 L. S. Rothman, The Hitran molecular database, Hawks, 1996.
24 M. Baranger, *Phys. Rev.*, 1958, **111**, 481; M. Baranger, *Phys. Rev.*, 1958, **111**, 494; M. Baranger, *Phys. Rev.*, 1958, **112**, 855.
25 U. Fano, *Phys. Rev.*, 1963, **131**, 259.
26 A. Ben-Reuven, *Phys. Rev.*, 1966, **141**, 34; A. Ben-Reuven, *Phys. Rev.*, 1966, **145**, 7.
27 R. Shafer and R. G. Gordon, *J. Chem. Phys.*, 1973, **58**, 5422.
28 J. P. Faroux, Thesis, CNRS Paris, 1969.
29 U. Fano and D. Dill, *Phys. Rev. A*, 1972, **6**, 185; E. S. Chang and U. Fano, *Phys. Rev. A*, 1972, **6**, 173.
30 A. Omont, *Prog. Quant. Electron.*, 1977, **5**, 69.
31 Ph. Brechignac, A. Picard-Bersellini, R. Charneau and J. M. Launay, *Chem. Phys.*, 1980, **53**, 165.
32 E. W. Smith, M. Giraud and J. Cooper, *J. Chem. Phys.*, 1976, **65**, 1256.
33 R. Blackmore, S. Green and L. Monchick, *J. Chem. Phys.*, 1988, **88**, 4113.
34 R. A. Brownsword, J. S. Salh and I. W. M. Smith, *J. Chem. Soc., Faraday Trans.*, 1995, **91**, 191.
35 D. R. Flower, G. Bourhis and J. M. Launay, *Comput. Phys. Commun.*, 2000, **131**, 187.
36 B. R. Johnson, *J. Chem. Phys.*, 1978, **69**, 4678.
37 R. K. Brimacombe and J. Reid, *IEEE J. Quant. Electron.*, 1983, **QE-19**, 1668.
38 P. M. Agrawal and L. M. Raff, *J. Chem. Phys.*, 1981, **75**, 2163.
39 D. C. Clary, *J. Chem. Phys.*, 1983, **78**, 4915.
40 A. E. DePristo and H. Rabitz, *J. Chem. Phys.*, 1978, **69**, 902.
41 M. C. Herpin and P. Lallemand, *J. Quant. Spectrosc. Radiat. Transfer*, 1975, **15**, 779.
42 D. C. Flatin, T. M. Goyette, M. M. Beaky, C. D. Ball and F. C. De Lucia, *J. Chem. Phys.*, 1999, **110**, 2087.